Available online at www.sciencedirect.com
ScienceDirect
Advances in Space Research 42 (2008) 1670–1675
ADVANCES IN SPACE RESEARCH (a COSPAR publication)
www.elsevier.com/locate/asr

Cosmic-ray electron spectrum above 100 GeV from PPB-BETS experiment in Antarctica

K. Yoshida [a,*], S. Torii [b], T. Yamagami [c], T. Tamura [d], H. Kitamura [e], J. Chang [f], I. Iijima [c], A. Kadokura [g], K. Kasahara [a], Y. Katayose [h], T. Kobayashi [i], Y. Komori [j], Y. Matsuzaka [c], K. Mizutani [k], H. Murakami [l], M. Namiki [c], J. Nishimura [c], S. Ohta [c], Y. Saito [c], M. Shibata [h], N. Tateyama [d], H. Yamagishi [g], T. Yuda [d]

[a] *Department of Electronic Information Systems, Shibaura Institute of Technology, 307 Fukasaku, Minuma-ku, Saitama-shi 337-8570, Japan*
[b] *Advanced Research Institute for Science and Engineering, Waseda University, 3-4-1 Okubo, Shinjuku-ku, Tokyo 169-8555, Japan*
[c] *Institute of Space and Astronautical Science, JAXA, 3-1-1 Oshinodai, Sagamihara 229-8510, Japan*
[d] *Institute of Physics, Kanagawa University, 3-27-1 Rokkakubashi, Kanagawa-ku, Yokohama 221-8686, Japan*
[e] *National Institute of Radiological Sciences, 4-9-1 Anagawa, Inage-ku, Chiba-shi 263-8555, Japan*
[f] *Purple Mountain Observatory, Chinese Academy of Sciences, 2 West Beijing Road, Nanjing 210008, China*
[g] *National Institute of Polar Research, 1-9-10 Kaga, Itabashi-ku, Tokyo 173-8515, Japan*
[h] *Department of Physics, Yokohama National University, 79-1 Tokiwadai, Hodogaya-ku, Yokohama 240-8501, Japan*
[i] *Department of Physics and Mathematics, Aoyama Gakuin University, 5-10-1 Fuchinobe, Sagamihara 229-8558, Japan*
[j] *Kanagawa University of Human Services, 1-10-1 Heiseicho, Yokosuka 238-8522, Japan*
[k] *Department of Physics, Saitama University, 255 Shimo-Okubo, Sakura-ku, Saitama-shi 338-8570, Japan*
[l] *Department of Physics, Rikkyo University, 3-34-1 Nishi-Ikebukuro, Toshima-ku, Tokyo 171-8501, Japan*

Received 15 December 2006; received in revised form 10 April 2007; accepted 12 April 2007

Abstract

Cosmic-ray electrons have been observed in the energy region from 10 GeV to 1 TeV with the PPB-BETS by a long duration balloon flight using a Polar Patrol Balloon (PPB) in Antarctica. The observation was carried out for 13 days at an average altitude of 35 km in January 2004. The PPB-BETS detector is an imaging calorimeter composed of scintillating-fiber belts and plastic scintillators inserted between lead plates. In the study of cosmic-ray electrons, there have been some suggestions that high-energy electrons above 100 GeV are a powerful probe to identify nearby cosmic-ray sources and search for particle dark matter. In this paper, we present the energy spectrum of cosmic-ray electrons in the energy range from 100 GeV to 1 TeV at the top of atmosphere, and compare our spectrum with the results from other experiments.

Keywords: Long duration balloon; Cosmic-ray electrons; Cosmic-ray origin

1. Introduction

Compared to cosmic-ray nuclei, high-energy electrons lose energy rapidly by the synchrotron and inverse Compton processes during propagation in the Galaxy. Because of these radiative losses, the high-energy electrons from the distant sources cannot reach the solar system. Hence, it has been suggested that the energy spectrum of cosmic-ray electrons might have a structure in the energy region above several 100 GeV due to the discrete effect of nearby supernova remnants (SNRs) (Kobayashi et al., 2004). This means that we can identify cosmic-ray electron sources from the electron spectrum above several 100 GeV together with anisotropies in arrival direction. In addition, there is a

* Corresponding author.
E-mail address: yoshida@shibaura-it.ac.jp (K. Yoshida).

0273-1177/$34.00
doi:10.1016/j.asr.2007.04.043

possibility that Weakly Interacting Massive Particles (WIMPs) annihilate directly into electron–positron pairs and produce mono-energetic electrons and positrons (Cheng et al., 2002). Although the propagation through the Galaxy would broaden the line spectrum, the observed electron and positron spectrum could still have a distinctive feature. Since there are no other known production mechanisms that would produce an electron and positron peak at energies of 100 GeV–10 TeV, such a distinctive feature clearly indicates the existence of WIMP dark matter in the Galactic halo. The observations of high-energy electrons bring us unique information about sources and propagation of cosmic rays, and enable us to search for WIMP dark matter.

However, the intensity of cosmic-ray electrons is ~1% of the protons at 10 GeV, and decreases very rapidly with energy at ~0.1% of protons at 1 TeV. This is due to the energy spectrum of electrons that shows a power law with the index of $-3.0 \sim 3.3$, which is steeper than that of protons with the index of -2.7. The electron observations require, particularly at energies over 100 GeV, the capability of high rejection power against the protons and long exposures with a detector that has a large geometrical factor. Because of these reasons, except for the emulsion chambers, it was difficult for many kinds of detectors to observe electrons over 100 GeV. Recently, ATIC-2, which is a balloon experiment over Antarctica, has achieved the electron observations in the energy region from 20 GeV to 1 TeV.

For observing cosmic-ray electrons above 10 GeV, we developed an imaging calorimeter, Balloon-borne Electron Telescope with Scintillating fibers (BETS), for the balloon experiment (Torii et al., 2000). We had successful observations of electrons at Sanriku in Japan, and derived the electron spectrum in the energy range from 10 GeV to 100 GeV (Torii et al., 2001). By improving the BETS instrument, we also observed atmospheric gamma rays in the energy range from a few GeV to several 10 GeV at mountain and at balloon altitudes for the calibration of the atmospheric neutrino flux calculations (Kasahara et al., 2002). In order to observe the higher-energy electrons above 100 GeV, we have developed an advanced BETS detector (Torii et al., 2006b) and observed cosmic-ray electrons by using Polar Patrol Balloon (PPB), which has a capability to achieve a long duration balloon flight for ~4 weeks at an altitude of ~35 km in Antarctica (Kadokura et al., 2002).

In this paper, we present the result of high-energy electron observations above 100 GeV with PPB-BETS.

2. Observations

Since the PPB-BETS instrument and the observation in Antarctica are described in detail in a previous paper (Torii et al., 2006b), we will briefly summarize the PPB-BETS detector and the observations.

The PPB-BETS detector consists of 36 scintillating fiber belts, 9 plastic scintillation counters, and 14 lead plates with a total thickness of 9 radiation lengths (r.l.). Each fiber belt is composed of 280 fibers with a 1 mm square cross section and the number of fibers is 10,080 in total. The basic structure is similar to that of the BETS detector (Torii et al., 2001), but several improvements have been adopted to observe high-energy electrons up to 1 TeV as described in the following paragraph.

The total thickness of lead is enlarged from 7 to 9 r.l., and the number of plastic scintillators used for the event-trigger and energy measurement is increased from 3 to 9 to carry out proton background rejection more effectively on-board. The image intensifier and CCD system for the read-out of scintillating fibers were considerably improved to avoid the saturation effects of image intensities up to a 1 TeV electron shower. The performance of the PPB-BETS detector was examined by a balloon experiment of the trigger system flown at Sanriku in Japan, beam tests of the flight model at the CERN-SPS by using electrons from 10 GeV to 200 GeV and protons from 150 GeV to 350 GeV, and Monte-Carlo simulations.

The balloon was launched at the Syowa Station (39.60°E, 69.01°S) in Antarctica at 15:57 on January 4, 2004 (UTC). The level flight was started at two hours after the launch and continued till 1:46 on January 17, 2004 at an average altitude of ~35 km. The total exposure time was 296 h. During the observations, the following new systems operated successfully: power supply system by solar panels, telemetry system by the Iridium satellite phone line, and auto-level control system by CPU.

Event trigger was executed by two modes, the low-energy (LE) mode and the high-energy (HE) mode. The LE mode corresponds to electron observation above 10 GeV and was assigned for the observation during the 10 h just after launching. The data acquired by the LE mode were directly transmitted to the Syowa Station with a bit rate of 64 kbps. The HE mode corresponds to electron observation above 100 GeV and was adopted throughout the flight duration. The data acquired by the HE mode were transmitted to our operation room at the National Institute of Polar Research (NIPR) in Japan, via a receiving station in the US, with the Iridium satellite phone line at a rate of 2.4 kbps. The number of acquired events was 2.2×10^4 for the LE mode with a trigger rate of ~3 Hz, and 5.7×10^3 for the HE mode with a trigger rate of ~0.02 Hz.

3. Data analysis

3.1. Data sets for analysis

For the event triggering the HE mode, we adopted two main sets of discrimination levels of pulse heights in all these plastic scintillators. One set corresponds to the threshold energy of 100 GeV and the other to 150 GeV. The number of acquired events is 3.1×10^3 for the 100 GeV threshold and 1.6×10^3 for the 150 GeV threshold. There are also 1.0×10^3 events for the other thresholds

on the HE mode. In this analysis, we used the two data sets of the 100 GeV and 150 GeV threshold without use of the other data including the LE mode. Fig. 1 shows the pulse height (converted to the number of Minimum Ionizing Particle, MIP) distribution of the plastic scintillator at the depth of 7 r.l. for the two thresholds. As shown in Fig. 1, the observable minimum energy is shifted properly depending on each threshold, and the trigger system worked normally. The spectra in high-energy region are compared to a power-law spectrum with an index of −2.7. They are consistent with the spectral shape of the cosmic-ray protons, since the events triggered on-board are still dominated by the protons that are much more abundant than the electrons.

3.2. Electron selection

For the acquired events, we reconstructed the raw CCD images of showers to the fiber positions in detector space by using the positions of each fiber on the CCD image. The positions of each fiber were obtained in advance of the flight by observing cosmic-ray muon tracks at ground level. The relative displacement of the fiber positions during the flight was calibrated by using the LED-illuminated fibers.

We applied an imaging analysis to select the electrons from the background particles as used in the analysis of BETS (Torii et al., 2001). We selected the events whose shower axes pass through the top and bottom of the detector within a zenith angle of 30°. This selection reduces the proton background events triggered on-board, which are incident from the side of the detector. A typical event of electron-induced shower presents a narrower lateral spread concentrated along the shower axis. On the contrary, that of proton-induced shower shows a wider lateral spread (Torii et al., 2006b). We characterize this physical property by the RE parameter, the ratio of energy deposition within 5 mm from the shower axis to the total, as described in Torii et al. (2001). Fig. 2 shows the RE distributions of the observed events compared with the distribution of 100 GeV electron and 250 GeV proton beams at CERN-SPS. The electron candidates were selected by the RE distribution under the condition that the RE values are greater than 0.75.

As for the separation between electrons and gamma rays, electrons could be identified by the presence of hits in the scintillating fibers at 0 r.l. along the shower axis. Fig. 3 presents the observed and simulated distributions of the distances of the nearest hit fiber position from the shower axis at the top layer. As incident electrons leave signals on the fibers along the shower axis, the distribution of electrons is concentrated around the incident point. On the other hand, as incident gamma rays leave no signals except for the back-scattered particles, the distribution by gamma rays becomes much broader. We judged electrons as the events whose distances are less than or equal to 5 mm. Gamma-ray events are rejected by 90%. As a result, the number of the electron candidates above 100 GeV is 84 events among the 4.7×10^3 analyzed events in the HE mode.

3.3. Energy measurements

Since the number of shower particles at the shower maximum is nearly proportional to the energy of incident electrons, we determined the electron energies by using the number of particles at the shower maximum in the transition curve with plastic scintillators. The transition curves of electro-magnetic shower are well represented by the following formula:

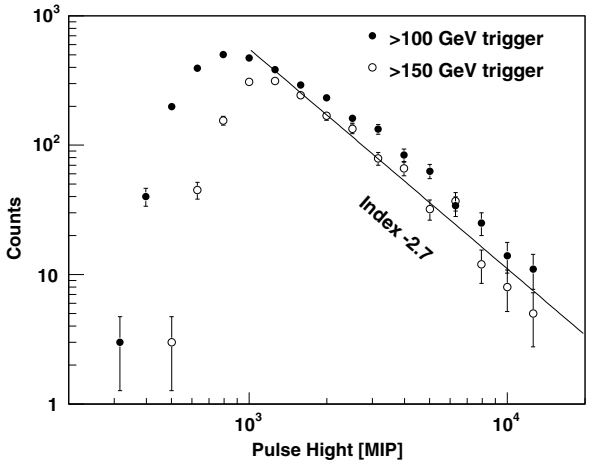

Fig. 1. Pulse height distributions of the plastic scintillator at the depth of 7 r.l. for the 100 GeV threshold (solid circles) and 150 GeV threshold (open circles). The solid line shows a power-law spectrum with an index of −2.7.

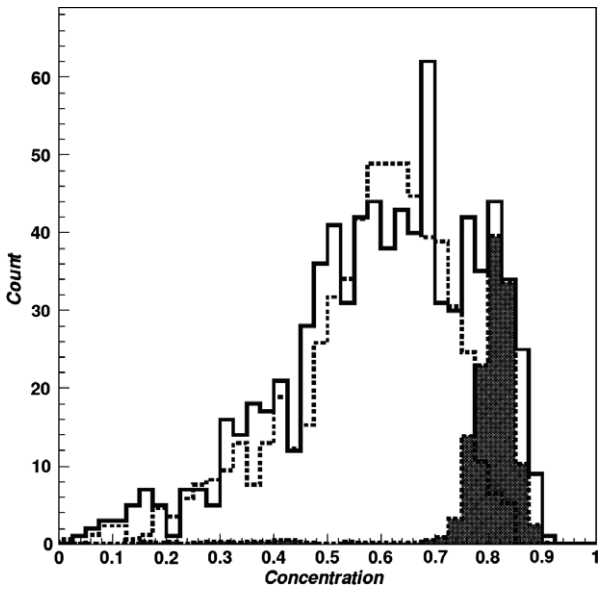

Fig. 2. RE distributions of the observed events (solid line) with 100 GeV electrons (hatched region) and 250 GeV protons (dashed line) of the CERN-SPS beam tests.

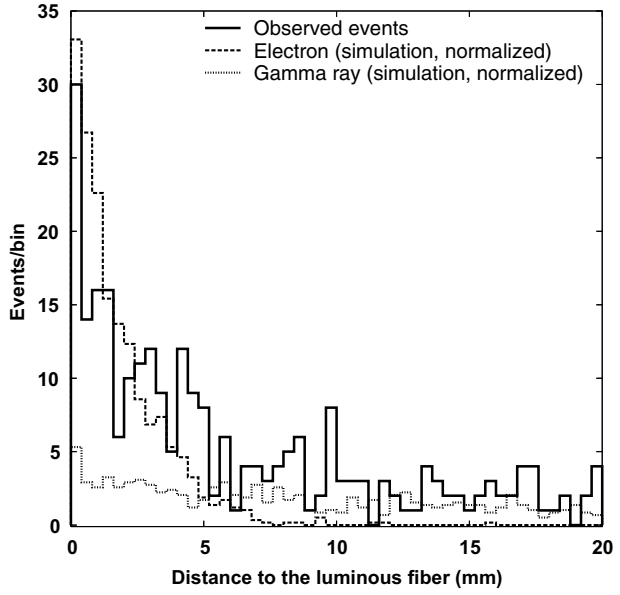

Fig. 3. Observed distribution of the nearest hit fiber positions from the shower axis (solid line) compared with the simulated distributions of electrons and gamma rays.

$$S = N\left(\frac{bt}{\cos\theta}\right)^{a-1}\exp\left(-\frac{bt}{\cos\theta}\right), \tag{1}$$

where S is the pulse heights (converted to MIP) of plastic scintillators at the depth of t r.l., N is the normalization factor, θ is the zenith angle of the shower axis, and a and b are adjustable coefficients. In order to derive the number of particles at the shower maximum, we fitted this formula to the pulse heights of the six scintillators at depths of 3–9 r.l. As shown in Fig. 4, the relation of the number of particles at the shower maximum and the energies of electron beams at CERN-SPS is almost linear in the energy range of 10–200 GeV. The energy resolution is 12% at 100 GeV as shown in Fig. 5, and consistent with the simulations.

3.4. Electron energy spectrum

From the electron events, with the above selection and energy determination, we derived the cosmic-ray electron spectrum by using the following formula:

$$J_e(E) = \left(\frac{N_e C_{RE} C_{eg}}{S\Omega T \Delta E} C_{enh} - C_{2nd}\right) C_{atm}, \tag{2}$$

where N_e is the number of electron candidates, $S\Omega$ the effective geometrical factor, T the observed live time, ΔE the energy interval, C_{RE} the correction factor of the proton contamination in the RE-cut with energy dependence, C_{eg} the correction factor of the gamma-ray contamination in the gamma-ray rejection with energy dependence, C_{enh} the correction of enhancement of flux due to the energy resolution, C_{2nd} the flux of secondary (atmospheric) electrons at the observation level, and C_{atm} the correction factor of energy loss of primary electrons in the overlying atmosphere.

The uncertainty of the energy determination has the effect of enhancing the absolute flux of electrons, in particular, for a steep power-law spectrum. We derived the enhancement factor C_{enh} above 100 GeV of 0.98 due to the energy resolution presented in Fig. 5.

In order to derive the primary electron spectrum, we subtracted the secondary electrons produced by the interactions of cosmic-ray nuclei. The energy spectrum of the estimated atmospheric electrons are represented by

$$C_{2nd}(E) = 1.32 \times 10^{-5}\left(\frac{E}{100\text{GeV}}\right)^{-2.73} (\text{m}^{-2}\,\text{s}^{-1}\,\text{sr}^{-1}\,\text{GeV}^{-1}) \tag{3}$$

at the altitude of 7.4 g cm^{-2} (Nishimura et al., 1980; Yoshida et al., 2006).

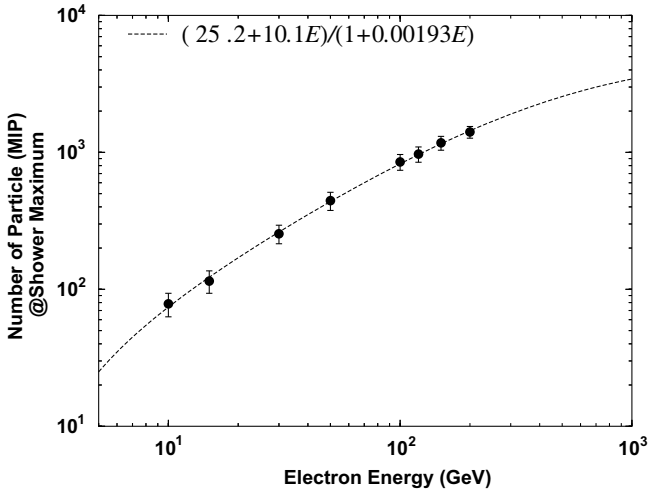

Fig. 4. Relation of the electron energy and the number of shower particles at the shower maximum by the CERN-SPS beam tests. The incident direction is perpendicular to the detector surface.

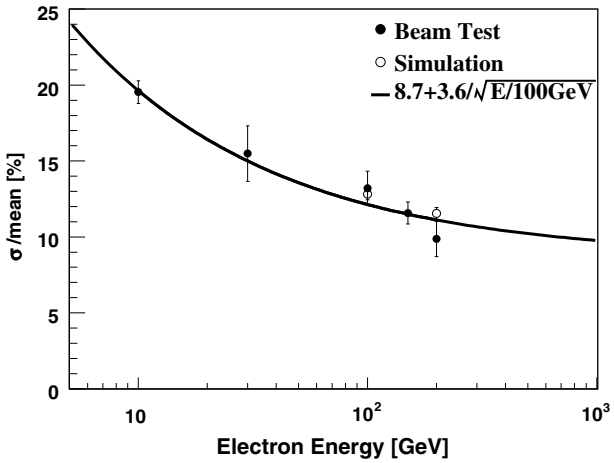

Fig. 5. Energy dependence of the energy resolution for the CERN-SPS electron beams with simulations. The incident direction is perpendicular to the detector surface.

The atmospheric correction factor, $C_{\rm atm}$, is caused by bremsstrahlung energy losses of the primary electrons. In the case of a single power-law spectrum with an index of $-\gamma$, the energy-loss correction due to the overlying atmosphere is given by $\alpha = e^{A(\gamma-1)t/(\gamma-1)}$, where t is the depth in r.l., and the notation A refers to the formula used in electro-magnetic shower theory (Nishimura et al., 1980). The energy-loss correction, α, corresponds to the correction factor of flux as follows: $C_{\rm atm} = \alpha^{\gamma-1}$. In the case of $\gamma = 3.0$ and 7.4 g cm^{-2} depth, the atmospheric correction factor is $C_{\rm atm} = 1.37$ for $\alpha = 1.17$.

From the raw numbers of electron candidates, we evaluated the electron numbers by correcting the proton contamination in the RE cut and the gamma-ray contamination in the gamma-ray rejection. Since the power-law index of the primary proton spectrum is -2.7, which is much harder than that of the electrons, the contamination of protons increases with energy. Atmospheric gamma rays are also produced by the interaction of primary protons with atmospheric nuclei. Therefore, the index of gamma rays is the same with that of protons. This brings the same energy dependence for the contamination of gamma rays with the protons. Hence, the correction factors are estimated to be $C_{\rm RE} = 1 - 0.325 \times (E/100\ {\rm GeV})^{\gamma-2.7}$ for the proton contamination and $C_{\rm eg} = 1 - 0.176 \times (E/100\ {\rm GeV})^{\gamma-2.7}$ for the gamma-ray contamination from the Monte-Carlo simulations.

The geometrical factor, $S\Omega$, is derived by Monte-Carlo simulations under the same condition of the experiment. Fig. 6 shows the geometrical factor with electron energies for the 100 GeV threshold and 150 GeV threshold in the HE mode.

4. Results and discussion

Fig. 7 presents the electron energy spectrum multiplied by the cube of energy, in comparison with other electron observations (Tang, 1984; Golden et al., 1984; Boezio et al., 2000; DuVernois et al., 2001; Torii et al., 2001; Aguilar et al., 2002; Kobayashi et al., 2002; Chang et al., 2005). The PPB-BETS spectrum represented by a single power-law function is given by

$$J_{\rm e} = (1.83 \pm 0.65) \times 10^{-4} \left(\frac{E}{100\ {\rm GeV}}\right)^{-3.09\pm0.35} ({\rm m^{-2}\,s^{-1}\,sr^{-1}\,GeV^{-1}}). \quad (4)$$

Our spectrum agrees well with the extrapolated spectrum of the BETS (Torii et al., 2001) at 100 GeV, and is consistent with that of ATIC-2 (Chang et al., 2005) within statistical errors in the 100 GeV–1 TeV region.

The energy spectrum exceeding 100 GeV is crucial to detect the nearby SNRs as discussed by Kobayashi et al. (2004), and electron-positron pairs from Kaluza-Klein dark matter annihilations (Cheng et al., 2002). The data statistics of our results, however, are insufficient to discuss the details of the contribution of nearby SNRs and/or WIMP dark matter. For the future observations, we are planning to increase greatly our statistics by experiments such as CALET with the geometrical factor of nearly 1 m^2 sr and the observation time of 3 years on the International Space Station (Torii, 2006a). It is expected that CALET can detect these distinctive signatures from the nearby SNRs and WIMP annihilations (Yoshida et al., 2005).

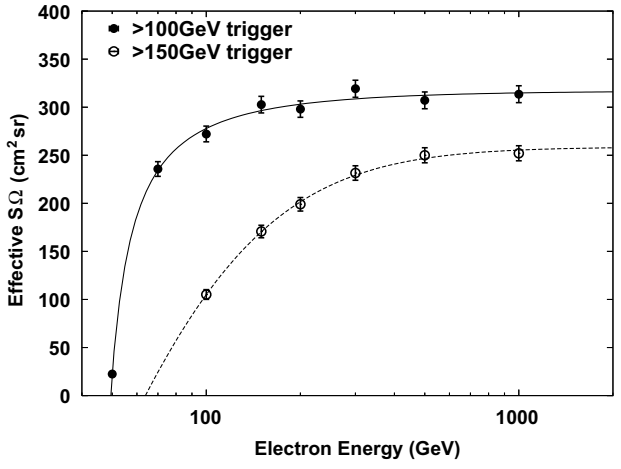

Fig. 6. The effective geometrical factor $S\Omega$ with the Monte-Carlo simulations under the same condition of the experiment.

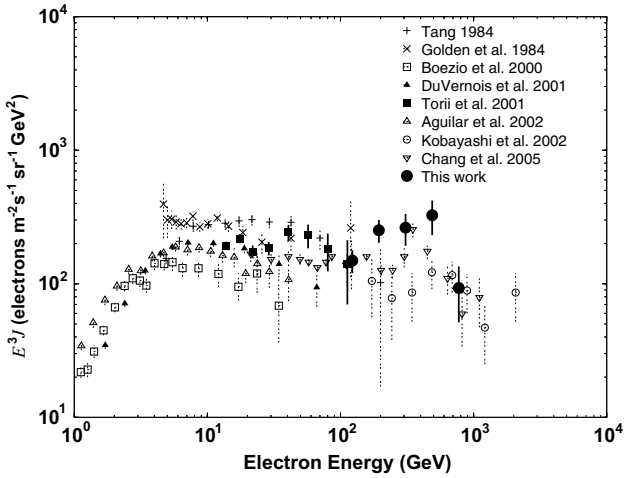

Fig. 7. Electron energy spectrum observed by the PPB-BETS (solid circles) in comparison with the energy spectra of other observations.

Acknowledgments

We sincerely thank the crew of the Syowa station in Antarctica and the Sanriku Balloon Center, ISAS/JAXA in Japan for their excellent and successful balloon flights. We also thank the staffs of the H4 beam line of CERN-SPS for their kind support. We are also grateful to D. Moen for his careful reading of the manuscript. This work was partly supported by Grants in Aid for Scientific Re-

search on Priority Area A (Grant No.14039212) and Scientific Research C (Grant Nos. 16540268, 18540293).

References

Aguilar, M., Alcaraz, J., Allaby, J., et al. The Alpha Magnetic Spectrometer (AMS) on the International Space Station: part I – results from the test flight on the space shuttle. Phys. Rep. 366, 331–405, 2002.

Boezio, M., Carlson, P., Francke, T., et al. The cosmic-ray electron and positron spectra measured at 1 AU during solar minimum activity. Astrophys. J. 532, 653–669, 2000.

Chang, J., Schmidt, W.K.H., Adams, J.H. et al. The electron spectrum above 20 GeV measured by ATIC-2, in: Proc. 29th ICRC, Pune, vol. 3, pp. 1–4, 2005.

Cheng, H.C., Feng, J.L., Matchev, K.T. Kaluza-Klein dark matter. Phys. Rev. Lett. 89, 211301-1–211301-4, 2002.

DuVernois, M.A., Barwick, S.W., Beatty, J.J., et al. Cosmic-ray electrons and positrons from 1 to 100 GeV: measurements with HEAT and their interpretation. Astrophys. J. 559, 296–303, 2001.

Golden, R.L., Mauger, B.G., Badhwar, G.D., et al. A measurement of the absolute flux of cosmic-ray electrons. Astrophys. J. 287, 622–632, 1984.

Kadokura, A., Yamagishi, H., Sato, N., et al. Polar patrol balloon experiment in Antarctica during 2002–2003. Adv. Polar Upper Atmos. Phys. 16, 157–172, 2002.

Kasahara, K., Mochizuki, E., Torii, S., et al. Atmospheric gamma-ray observation with the BETS detector for calibrating atmospheric neutrino flux calculations. Phys. Rev. D 66, 052004-1–052004-9, 2002.

Kobayashi, T., Komori, Y., Yoshida, K., et al. Observations of high-energy cosmic-ray electrons and atmospheric gamma rays with emulsion chambers. Uchuken Houkoku SP 44, 99–125, 2002.

Kobayashi, T., Komori, Y., Yoshida, K., Nishimura, J. The most likely sources of high-energy cosmic-ray electrons in supernova remnants. Astrophys. J. 601, 340–351, 2004.

Nishimura, J., Fujii, M., Taira, T., et al. Emulsion chamber observations of primary cosmic-ray electrons in the energy range 30–1000 GeV. Astrophys. J. 238, 394–409, 1980.

Tang, K.K. The energy spectrum of electrons and cosmic-ray confinement: a new measurement and its interpretation. Astrophys. J. 278, 881–892, 1984.

Torii, S., Tamura, T., Tateyama, N., et al. The balloon-borne electron telescope with scintillating fibers (BETS). Nucl. Instrum. Methods Phys. Res. A 452, 81–93, 2000.

Torii, S., Tamura, T., Tateyama, N., et al. The energy spectrum of cosmic-ray electrons from 10 to 100 GeV observed with a highly granulated imaging calorimeter. Astrophys. J. 559, 973–984, 2001.

Torii, S. for the CALET Collaboration CALET for high energy electron and gamma-ray measurements on ISS. Nucl. Phys. B (Proc. Suppl.) 150, 345–348, 2006a.

Torii, S., Yoshida, K., Tamura, T., Tateyama, N., et al. Study of >100 GeV electrons with BETS detector using a long duration balloon flight in Antarctica. Adv. Space Res. 37, 2095–2102, 2006b.

Yoshida, K., Torii, S., Tamura, T. et al. Observation of high-energy electron, gamma ray, and dark matter with CALET, high-energy cosmic-ray electrons beyond 100 GeV, in: Proc. of 29th ICRC, Pune, vol. 3, pp. 337–340, 2005.

Yoshida, K., Ohmori, R., Kobayashi, T., et al. Cosmic-ray spectra of primary protons and high altitude muons deconvolved from observed atmospheric gamma rays. Phys. Rev. D 74, 083511-1–083511-13, 2006.